Probing the Spin Pumping Mechanism: Exchange Coupling with Exponential Decay in $Y_3Fe_5O_{12}$/Barrier/Pt Heterostructures

C. H. Du,[1] H. L. Wang,[1] Y. Pu,[1] T. L. Meyer,[2] P. M. Woodward,[2] F. Y. Yang,[1,*] and P. C. Hammel[1,†]

[1]*Department of Physics, The Ohio State University, Columbus, Ohio 43210, USA*

[2]*Department of Chemistry and Biochemistry, The Ohio State University, Columbus, Ohio 43210, USA*

(Received 2 August 2013; published 11 December 2013)

It is widely believed that the mechanism for spin pumping in ferromagnet-nonmagnet bilayers is the exchange interaction between the ferromagnet and nonmagnetic material. We observe 1000-fold exponential decay of spin pumping from thin $Y_3Fe_5O_{12}$ films to Pt across insulating barriers, from which exponential decay lengths of 0.16, 0.19, and 0.23 nm are extracted for oxide barriers having band gaps of 4.91, 3.40, and 2.36 eV, respectively. This archetypal signature of quantum tunneling through a barrier underscores the importance of exchange coupling for spin pumping and reveals its dependence on the characteristics of the barrier material.

DOI: 10.1103/PhysRevLett.111.247202 PACS numbers: 75.47.Lx, 61.05.cp, 75.70.Ak, 76.50.+g

Generation and manipulation of spin currents is centrally important for spintronic applications [1]. Ferromagnetic resonance (FMR) driven spin pumping has been demonstrated to inject a pure spin current through angular momentum transfer from a ferromagnet (FM) to an adjacent nonmagnetic material (NM) [2–6]. It is generally believed that this dynamic coupling proceeds by means of the exchange interaction between the precessing magnetization ($\mathbf{M}$) of the FM and the conduction electrons of the NM at the NM-FM interface. This mechanism will lead to a short-range coupling that decays exponentially [2–7] on atomic length scales with separation between the FM and NM. However, this has not been experimentally confirmed, partially due to the large dynamic range needed to measure such a rapidly decaying spin pumping signal [6,8]. Our recent demonstration of large spin pumping in Pt/$Y_3Fe_5O_{12}$ (YIG) bilayers with mV-level inverse spin Hall effect (ISHE) voltage, V_{ISHE} [9], offers a material platform with signal-to-noise ratio sufficient to quantitatively characterize the coupling range, enabling detailed insight into the spin pumping mechanism. We report systematic measurements with four different barrier materials, including three oxide insulators and Si, to investigate the barrier thickness t dependence of spin pumping in Pt/barrier(t)/YIG heterostructures. We observe clear exponential decays of ISHE voltage with characteristic length scales of $\sim$0.2 nm for the oxide barriers; these data provide clear evidence for the predicted exchange coupling model for spin pumping.

Our experiments utilize YIG thin films grown on (111)-oriented $Gd_3Ga_5O_{12}$ (GGG) substrates by an off-axis sputtering technique we developed for epitaxial film growth of complex materials [9–13]. Figure 1(a) shows a high resolution x-ray diffraction (XRD) scan of a 20-nm YIG film near the YIG (444) peak with clear Laue oscillations, indicating high uniformity throughout the film. The XRD rocking curve in the inset to Fig. 1(a) taken at the 2θ value indicated by the arrow gives a full width at half maximum of 0.0185°, demonstrating excellent crystalline quality. Figure 1(b) shows a representative FMR derivative spectrum for a 20 nm YIG film taken at radio frequency (rf) $f = 9.65$ GHz and microwave power $P_{\mathrm{rf}} = 0.2$ mW with an in-plane magnetic field, from which the peak-to-peak linewidth (ΔH) of 10 Oe is obtained [14].

The spin pumping measurements are conducted at room temperature using a 5-nm thick Pt layer on 20-nm YIG films, as illustrated in Fig. 1(c). The samples ($\sim$ 1 mm wide and $\sim$5 mm long) are placed in the center of an FMR cavity and in a dc magnetic field ($\boldsymbol{H}$) applied in the xz plane. At resonance, the precessing magnetization transfers angular momentum from the YIG to the conduction electrons in Pt by means of dynamical coupling [6,15], generating a pure spin current $\boldsymbol{J}_s$ in Pt directed along the z axis with a polarization ($\boldsymbol{\sigma}$) parallel to the YIG magnetization. In the Pt layer, $\boldsymbol{J}_s$ is converted into a net charge current, $\boldsymbol{J}_c \propto \boldsymbol{J}_s \times \boldsymbol{\sigma}$, via the inverse spin Hall effect [16–19], resulting in an ISHE voltage V_{ISHE} along the y axis. Figure 1(d) shows V_{ISHE} vs H spectra for a Pt/YIG bilayer at $\theta_H = 90°$ and 270° (field in plane) at $P_{\mathrm{rf}} =$ 200 mW. The peak value of $V_{\mathrm{ISHE}} = 1.0$ mV is generated at the FMR resonant condition as illustrated by the FMR derivative spectrum in Fig. 1(e). As $\boldsymbol{H}$ is reversed from $\theta_H =$ 90° to 270°, V_{ISHE} changes sign and maintains the same magnitude as expected since $\boldsymbol{\sigma}$ changes sign with reversal of $\boldsymbol{M}$ ($\boldsymbol{M}$ is essentially parallel to $\boldsymbol{H}$ since H exceeds $4\pi M_s$ at resonance), resulting in a reversed sign of V_{ISHE}. The recently reported proximity effect in Pt/YIG bilayers [20–22] should contribute, at most, a μV-level signal to the measured V_{ISHE}, which is negligible compared with the observed mV-ISHE voltages in our Pt/YIG bilayers. In addition to YIG/Pt, we have also observed mV-level ISHE voltage in YIG/W [9] and YIG/Ta [23] bilayers.

Figure 1(f) shows the angular dependence of normalized $V_{\mathrm{ISHE}}(\theta_H)$ for the Pt/YIG bilayer, which agrees with the

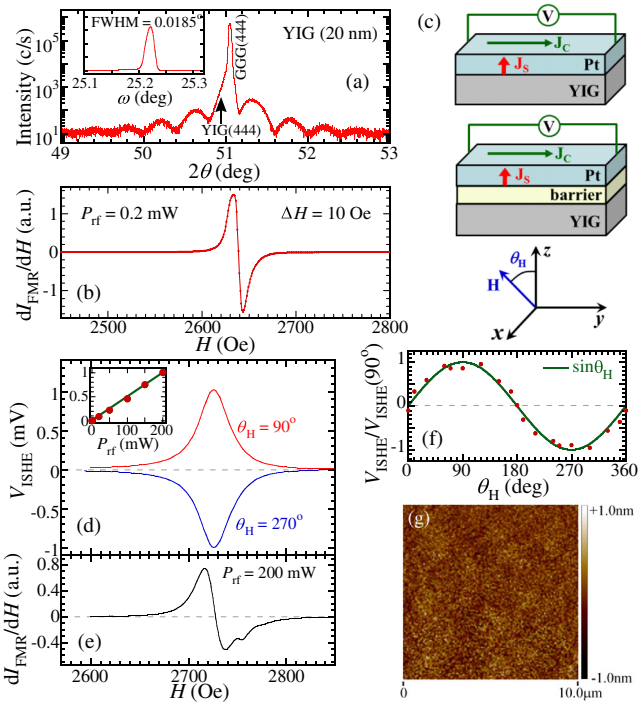

FIG. 1 (color online). (a) Semi-log θ-2θ XRD scan of a 20-nm thick YIG film on GGG (111), which exhibits clear Laue oscillations corresponding to the film thickness. Inset: rocking curve of the YIG (444) peak. (b) Representative room-temperature FMR derivative spectrum of a 20-nm YIG film with $\boldsymbol{H}$ in plane at $P_{\rm rf} = 0.2$ mW, which gives a peak-to-peak linewidth of 10 Oe. (c) Schematics of experimental setup for ISHE voltage measurements for Pt/YIG and Pt/barrier/YIG samples. (d) $V_{\rm ISHE}$ vs H spectra and (e) FMR derivative spectrum of a Pt(5 nm)/YIG(20 nm) bilayer at $P_{\rm rf} = 200$ mW. The inset in (d) is the rf power dependence of $V_{\rm ISHE}$ with a least-squares fit. (f) Angular dependence of normalized $V_{\rm ISHE}$ of the Pt/YIG bilayer (the green curve is a simple calculation of $\sin\theta_H$). (g) An AFM image of a 20-nm YIG film showing rms roughness of 0.15 nm over a 10 μm $\times$ 10 μm area.

expected $\sin\theta_H$ dependence (green curve), confirming that the observed voltage signal comes from FMR spin pumping,

$$V_{\rm ISHE} \propto \boldsymbol{J_s} \times \boldsymbol{\sigma} \propto \boldsymbol{J_s} \times \boldsymbol{M} \propto \boldsymbol{J_s} \times \boldsymbol{H} \propto \sin\theta_H. \quad (1)$$

The ISHE voltage of the Pt/YIG bilayer at $\theta_H = 90°$ is shown in the inset to Fig. 1(d) to be proportional to power $P_{\rm rf}$ for 0.2 mW $< P_{\rm rf} <$ 200 mW, indicating that the observed mV-level $V_{\rm ISHE}$ is in the linear regime. Figure 1(g) shows an atomic force microscopy (AFM) image of a 20-nm thick YIG film, which gives a root-mean-square (rms) roughness of 0.15 nm, corroborating the smooth surface as indicated by the Laue oscillations in Fig. 1(a) (see Supplemental Material [24] for more AFM characterization).

To study the coupling range of spin pumping, we insert four different thin, insulating barriers, Sr_2GaTaO_6 (SGTO) with a band gap $E_g = 4.91$ eV, $SrTiO_3$ (STO) with $E_g = 3.40$ eV [25,26], Sr_2CrNbO_6 (SCNO) with $E_g = 2.36$ eV and amorphous Si, between Pt and YIG as illustrated in Fig. 1(c) (see Supplemental Material [24] for detailed characteristics of the double perovskites Sr_2GaTaO_6 and Sr_2CrNbO_6). Figure 2 shows the spin pumping and FMR derivative absorption spectra of the Pt/barrier/YIG structures with 0.5-nm Sr_2GaTaO_6, $SrTiO_3$, Sr_2CrNbO_6 and Si barriers; these barriers reduce the ISHE voltage to 20, 60, 100, and 440 μV, respectively. We discuss this variation of the decay rate of $V_{\rm ISHE}$ below.

The insets on the left in Figs. 2(a)–2(d) show the angular dependencies of the normalized $V_{\rm ISHE}$ for Pt/barrier(0.5 nm)/YIG with the four barriers. The sinusoidal angular dependence is characteristic of the ISHE [see Eq. (1)], confirming that the observed signals are due to spin pumping, not artifacts due to thermoelectric or magnetoelectric effects such as anisotropic magnetoresistance [20,27]. The insets on the right in Figs. 2(a)–2(d) show the rf power dependencies of $V_{\rm ISHE}$ from $P_{\rm rf} = 0.2$ to 200 mW with an in-plane field ($\theta_H = 90°$) for the four samples; all show a linear relationship between $P_{\rm rf}$ and $V_{\rm ISHE}$ [28].

The systematic behavior of spin pumping across a thin insulating barrier becomes evident when the dependencies

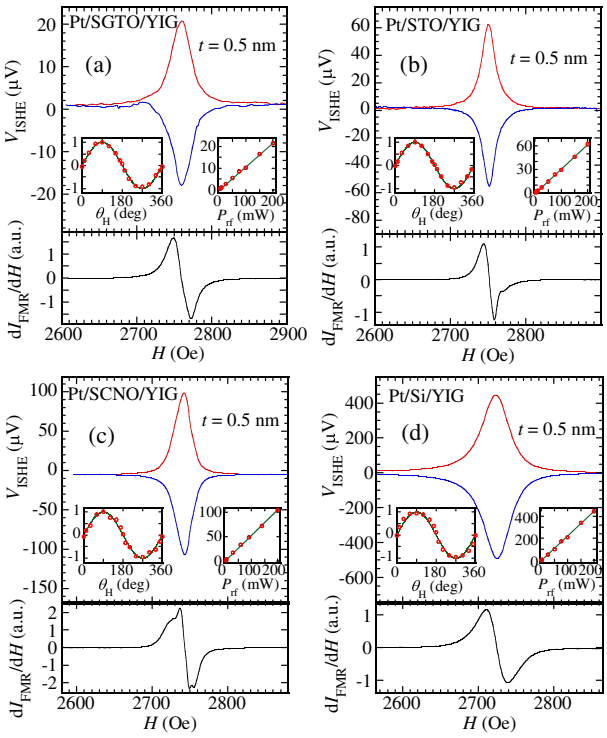

FIG. 2 (color online). $V_{\rm ISHE}$ vs H (upper panel) and the corresponding FMR derivative spectra (lower panel) of Pt/barrier/YIG multilayers with 0.5-nm thick (a) Sr_2GaTaO_6, (b) $SrTiO_3$, (c) Sr_2CrNbO_6, and (d) Si barriers at $P_{\rm rf} =$ 200 mW. The left inset in each upper panel shows the angular dependence of the normalized $V_{\rm ISHE}$ which exhibits the expected $\sin\theta_H$ (green curves) dependence on θ_H, and the right inset shows the rf power dependence of $V_{\rm ISHE}$.

of V_{ISHE} (normalized by the Pt/YIG samples with direct contact) on the barrier thickness are plotted as shown in Figs. 3(a)–3(d) for the Pt/barrier(t)/YIG heterostructures with Sr_2GaTaO_6, $SrTiO_3$, Sr_2CrNbO_6, and Si barriers. Four representative V_{ISHE} vs H spectra for various barrier thicknesses are shown in Figs. 3(e)–3(h) for each series. The mV-scale ISHE voltage of Pt/YIG allows us to observe dramatic, 1000-fold changes in V_{ISHE}. As the barrier thickness increases, V_{ISHE} exhibits a clear exponential decay for all three barrier materials and eventually falls below the noise level at $t = 2$ nm for the Sr_2GaTaO_6, $SrTiO_3$, and Sr_2CrNbO_6 barriers and at $t = 5$ nm for the Si barrier. From a least-squares fit shown in the semi-log plots in Figs. 3(a)–3(d), we obtain an exponential decay length $\lambda = 0.16$, 0.19, 0.23, and 0.74 nm for the Sr_2GaTaO_6, $SrTiO_3$, Sr_2CrNbO_6, and Si barriers, respectively, following

$$V_{ISHE} = V_{ISHE}(t = 0)e^{-t/\lambda}. \quad (2)$$

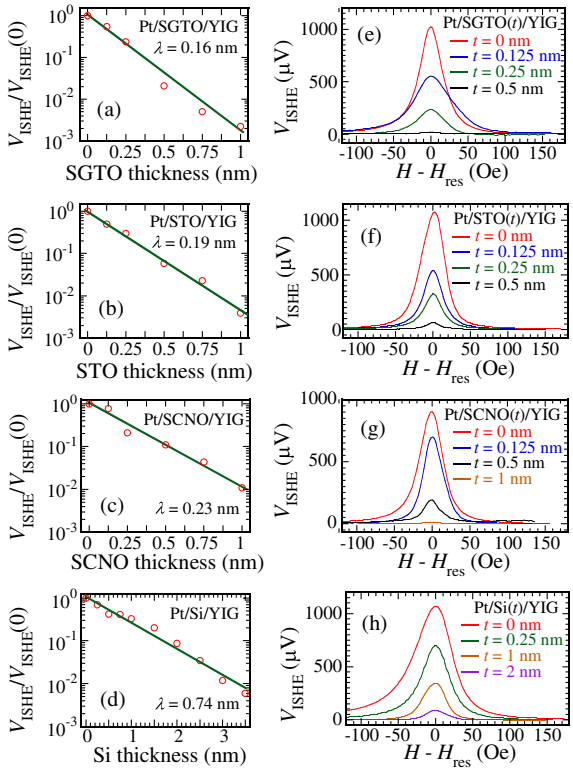

FIG. 3 (color online). Semi-log plots of V_{ISHE} normalized to the values for Pt/YIG bilayers with direct contact as a function of the barrier thickness of (a) Pt/Sr_2GaTaO_6/YIG, (b) Pt/$SrTiO_3$/YIG, (c) Pt/Sr_2CrNbO_6/YIG, and (d) Pt/Si/YIG, with four representative V_{ISHE} vs H spectra of various barrier thicknesses for each series shown in (e),(f),(g), and (h), respectively. The solid lines in (a), (b), (c), and (d) are least-squares fits, indicating the rate of exponential decay of ISHE voltages with decay length $\lambda = 0.16$, 0.19, 0.23, and 0.74 nm for Pt/Sr_2GaTaO_6/YIG, Pt/$SrTiO_3$/YIG, Pt/Sr_2CrNbO_6/YIG, and Pt/Si/YIG, respectively.

The spin current J_s is given by [19]

$$J_s = \frac{t_N \sigma_N}{\theta_{SH} \lambda_{SD} \tanh(\frac{t_N}{2\lambda_{SD}})} \frac{V_{ISHE}}{L}, \quad (3)$$

where σ_N, t_N, θ_{SH}, λ_{SD} are the conductivity, thickness, spin Hall angle, and spin diffusion length of the Pt layer, respectively. L is the sample length. Since $V_{ISHE} \propto J_s$, the exponential decay of V_{ISHE} indicates that the pure spin current generated in Pt also decreases exponentially with t, a signature behavior of exchange coupling between the FM and NM separated by an insulating barrier. This result provides the first direct, quantitative evidence of the exchange coupling model for spin pumping.

The exponential dependence of spin pumping on barrier thicknesses can be explained by a process in which the wave function of the conduction electrons in Pt tunnels through the barrier, couples with the precessing magnetization of YIG through exchange interaction, and acquires spin polarization via spin-dependent scattering at the barrier/YIG interface [2–5]. At a NM/FM interface, a spin current can be generated either by transmission of spin-polarized electrons from the FM into the NM, or by spin-dependent scattering of the conduction electrons in the NM at the interface. Given that YIG is an insulator, it is unlikely that spin-polarized electrons flow from YIG into Pt. This suggests that spin-dependent scattering of Pt conduction electrons at the Pt/YIG interface via the exchange interaction with the precessing magnetization of YIG is the dominant mechanism.

The ability of conduction electrons in Pt to tunnel through the barrier separating the Pt from the YIG will depend sensitively on the height of the energy barrier. At the interface between a metal and an insulator or a semiconductor, the relevant barrier is typically the Schottky barrier Φ_B, which depends on the work function of the metal and on the electron affinity, charge carrier type, and concentration of the insulator or semiconductor. Here we estimate the values of Φ_B for Pt/Sr_2GaTaO_6, Pt/$SrTiO_3$, and Pt/Sr_2CrNbO_6 based on published results on metal-perovskite Schottky junctions and correlate them with our measured decay lengths. The Schottky barrier height for Au on Nd-doped $SrTiO_3$ (carrier density 10^{17}–10^{18} cm^{-3}) Schottky junctions [29] is reported to be in the range 1.4–1.7 eV, about half of the $SrTiO_3$ band gap. At lower carrier concentration, Φ_B is expected to remain in this range. Our $SrTiO_3$ layers are highly resistive (beyond the instrument limit in our resistance measurements). Thus, the carrier density of our $SrTiO_3$ layers should be low. Au and Pt have similar work functions (5.47 eV for Au and 5.64 eV for Pt), so we expect Φ_B in Pt/$SrTiO_3$ to be around 1.7 eV (about half of the band gap). Since both Sr_2GaTaO_6 and Sr_2CrNbO_6 are also Sr-based perovskites [30], it is reasonable to expect Φ_B in Pt/Sr_2GaTaO_6 and Pt/Sr_2CrNbO_6 to be about half of their barrier band gaps as well. Using band gaps of 4.91 eV for Sr_2GaTaO_6 and 2.36 eV for Sr_2CrNbO_6

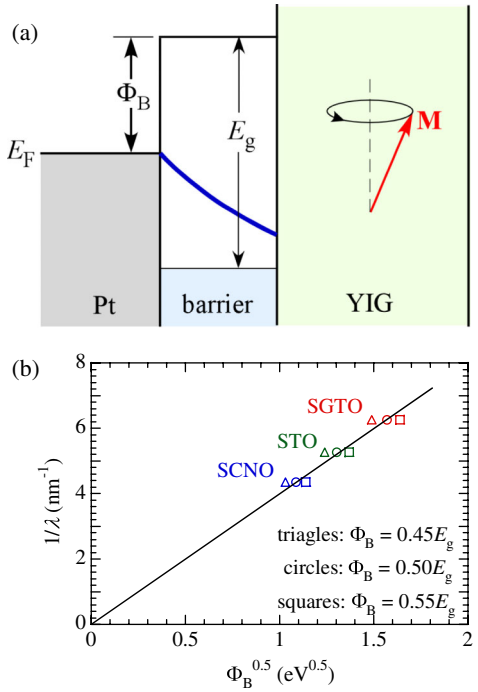

FIG. 4 (color online). (a) Schematic of band structures of Pt/barrier/YIG heterostructures with an estimated Schottky barrier height Φ_B at half of the band gap for each barrier material. The blue curve illustrates the quantum tunneling of the electron wave function from Pt into the barrier. (b) Inverse of decay length, $1/\lambda$, as a function of $\sqrt{\Phi_B}$ for Pt/Sr_2GaTaO_6/YIG, $Pt/SrTiO_3$/YIG, and Pt/Sr_2CrNbO_6/YIG, which includes three sets of values of $\Phi_B = 0.45E_g$ (triangles), $0.50E_g$ (circles), and $0.55E_g$ (squares). The solid line connecting the three points and origin is a guide to the eye.

determined by optical absorption (see Supplemental Material [24] for details) and the reported $E_g = 3.40$ eV for $SrTiO_3$ [25,26], we estimate $\Phi_B = 2.46$, 1.70, and 1.18 eV for Pt/Sr_2GaTaO_6, $Pt/SrTiO_3$, and Pt/Sr_2CrNbO_6 interfaces, respectively. To cover the possible range of Φ_B due to its sensitivity to a number of parameters, we also consider $\Phi_B = 0.45E_g$ and $0.55E_g$, which span a range of $\Phi_B = 2.21$–2.90, 1.53–1.87, and 1.06–1.30 eV for Pt/Sr_2GaTaO_6, $Pt/SrTiO_3$, and Pt/Sr_2CrNbO_6, respectively.

For a finite rectangular potential barrier, as illustrated in Fig. 4(a) for the three oxide barriers, the electron tunneling transmission coefficient D is determined by the barrier height Φ_B and width t [31]:

$$D \propto \exp\left[-\frac{2t}{\hbar}\sqrt{2m\Phi_B}\right], \tag{4}$$

where m is the effective electronic mass and $\hbar$ is Planck's constant. Since $V_{ISHE} \propto \boldsymbol{J}_s \propto D$, Eqs. (2) and (3) imply $1/\lambda \propto \sqrt{\Phi_B}$, as shown in Fig. 4(b) for Pt/Sr_2GaTaO_6/YIG, $Pt/SrTiO_3$/YIG, and Pt/Sr_2CrNbO_6/YIG. The experimental data points for the range of $\Phi_B = 0.45E_g$–$0.55E_g$ are quite consistent with a vanishing intercept, providing further evidence for the exchange coupling model in spin pumping and the role of barrier characteristics in quantum tunneling.

For Si barriers, the decay length of 0.74 nm is much larger than the 0.16, 0.19, and 0.23 nm for samples with oxide barriers. Si has a smaller band gap (1.1 eV) than the three oxide barriers; thus, we expect a larger decay length. If we use $\Phi_B = 0.55$ eV for Pt on amorphous Si, we estimate a decay length of 0.34 nm using the same rectangular potential barrier model, smaller than observed, indicating that, for Si, either the barrier height is not simply related to the band gap, or that the simple tunneling model used for oxide barriers is not adequate. This is not unexpected, however, since the Schottky barrier heights of metal and Si junctions are sensitive to the doping type and carrier concentration. In addition to the mechanism already discussed, we should also consider the possibility that there may be carriers in the Si barrier allowing either an indirect exchange process or spin diffusion through the barrier [32]. Further investigation of the characteristics of the barriers in spin pumping is needed to obtain better insights into the spin pumping mechanisms.

Experimental observation of a clear exponential decay of dynamic spin pumping provides clear evidence for, and quantitative understanding of a fundamental spin pumping mechanism. This result points to the important ability to tune characteristics of spin functional devices and reveal new phenomena.

This work is supported by the Center for Emergent Materials at the Ohio State University, a NSF Materials Research Science and Engineering Center (DMR-0820414) (H. L. W., Y. P., and F. Y. Y.) and by the Department of Energy through Grant No. DE-FG02-03ER46054 (P. C. H.). Partial support is provided by Lake Shore Cryogenics Inc. (C. H. D.) and the NanoSystems Laboratory at the Ohio State University. C. H. D. and H. L. W. made equal contributions to this work.

*fyyang@physics.osu.edu
†hammel@physics.osu.edu

[1] I. Žutić, J. Fabian, and S. Das Sarma, Rev. Mod. Phys. **76**, 323 (2004).
[2] Y. Tserkovnyak, A. Brataas, and G. E. W. Bauer, Phys. Rev. Lett. **88**, 117601 (2002).
[3] A. A. Kovalev, A. Brataas, and G. E. W. Bauer, Phys. Rev. B **66**, 224424 (2002).
[4] Y. Tserkovnyak, A. Brataas, and G. E. W. Bauer, Phys. Rev. B **66**, 224403 (2002).
[5] Y. Tserkovnyak, A. Brataas, G. E. W. Bauer, and B. I. Halperin, Rev. Mod. Phys. **77**, 1375 (2005).
[6] Y. Kajiwara, K. Harii, S. Takahashi, J. Ohe, K. Uchida, M. Mizuguchi, H. Umezawa, H. Kawai, K. Ando, K.

Takanashi, S. Maekawa, and E. Saitoh, Nature (London) **464**, 262 (2010).
[7] S. S. P. Parkin, Phys. Rev. Lett. **71**, 1641 (1993).
[8] O. Mosendz, J. Pearson, F. Fradin, S. Bader, and A. Hoffmann, Appl. Phys. Lett. **96**, 022502 (2010).
[9] H. L. Wang, C. H. Du, Y. Pu, R. Adur, P. C. Hammel, and F. Y. Yang, Phys. Rev. B **88**, 100406(R) (2013).
[10] A. J. Hauser, R. E. A. Williams, R. A. Ricciardo, A. Genc, M. Dixit, J. M. Lucy, P. M. Woodward, H. L. Fraser, and F. Y. Yang, Phys. Rev. B **83**, 014407 (2011).
[11] A. J. Hauser, J. R. Soliz, M. Dixit, R. E. A. Williams, M. A. Susner, B. Peters, L. M. Mier, T. L. Gustafson, M. D. Sumption, H. L. Fraser, P. M. Woodward, and F. Y. Yang, Phys. Rev. B **85**, 161201(R) (2012).
[12] C. H. Du, R. Adur, H. L. Wang, A. J. Hauser, F. Y. Yang, and P. C. Hammel, Phys. Rev. Lett. **110**, 147204 (2013).
[13] A. J. Hauser, J. M. Lucy, H. L. Wang, J. R. Soliz, A. Holcomb, P. Morris, P. M. Woodward, and F. Y. Yang, Appl. Phys. Lett. **102**, 032403 (2013).
[14] M. Farley, Rep. Prog. Phys. **61**, 755 (1998).
[15] B. Heinrich, C. Burrowes, E. Montoya, B. Kardasz, E. Girt, Y.-Y. Song, Y. Y. Sun, and M. Z. Wu, Phys. Rev. Lett. **107**, 066604 (2011).
[16] E. Saitoh, M. Ueda, H. Miyajima, and G. Tatara, Appl. Phys. Lett. **88**, 182509 (2006).
[17] S. O. Valenzuela and M. Tinkham, Nature (London) **442**, 176 (2006).
[18] K. Ando, S. Takahashi, J. Ieda, H. Kurebayashi, T. Trypiniotis, C. H. W. Barnes, S. Maekawa, and E. Saitoh, Nat. Mater. **10**, 655 (2011).
[19] K. Ando *et al.*, J. Appl. Phys. **109**, 103913 (2011).
[20] S. Y. Huang, X. Fan, D. Qu, Y. P. Chen, W. G. Wang, J. Wu, T. Y. Chen, J. Q. Xiao, and C. L. Chien, Phys. Rev. Lett. **109**, 107204 (2012).
[21] Y. Y. Sun, H. C. Chang, M. Kabatek, Y.-Y. Song, Z. H. Wang, M. Jantz, W. Schneider, M. Z. Wu, E. Montoya, B. Kardasz, B. Heinrich, S. G. E. te Velthuis, H. Schultheiss, and A. Hoffmann, Phys. Rev. Lett. **111**, 106601 (2013).
[22] Y. M. Lu, Y. Choi, C. M. Ortega, X. M. Cheng, J. W. Cai, S. Y. Huang, L. Sun, and C. L. Chien, Phys. Rev. Lett. **110**, 147207 (2013).
[23] H. L. Wang, C. H. Du, Y. Pu, R. Adur, P. C. Hammel, and F. Y. Yang, arXiv:1307.2648.
[24] See Supplemental Material at http://link.aps.org/supplemental/10.1103/PhysRevLett.111.247202 for details of film deposition, oxide band gap measurements, and AFM results.
[25] G. A. Barbosa, R. S. Katiyar, and S. P. S. Porto, J. Opt. Soc. Am. **68**, 610 (1978).
[26] M. N. Kamalasanan, N. D. Kumar, and S. Chandra, J. Appl. Phys. **74**, 679 (1993).
[27] M. Harder, Z. X. Cao, Y. S. Gui, X. L. Fan, and C.-M. Hu, Phys. Rev. B **84**, 054423 (2011).
[28] M. V. Costache, M. Sladkov, S. M. Watts, C. H. van der Wal, and B. J. van Wees, Phys. Rev. Lett. **97**, 216603 (2006).
[29] T. Shimizu and H. Okushi, J. Appl. Phys. **85**, 7244 (1999).
[30] D. R. Lide, *Handbook of Chemistry and Physics* (CRC Press, Taylor & Francis Group, New York, 2005), 86th ed..
[31] R. Shankar, *Principles of Quantum Mechanics* (Springer, New York, 1994), 2nd ed..
[32] E. Shikoh, K. Ando, K. Kubo, E. Saitoh, T. Shinjo, and M. Shiraishi, Phys. Rev. Lett. **110**, 127201 (2013).